Atmospheric Environment 112 (2015) 294–305

Contents lists available at ScienceDirect

Atmospheric Environment

journal homepage: www.elsevier.com/locate/atmosenv

Simulating the transport and chemical evolution of biomass burning pollutants originating from Southeast Asia during 7-SEAS/2010 Dongsha experiment

Ming-Tung Chuang [a, *], Joshua S. Fu [b], Neng-Huei Lin [c], Chung-Te Lee [d], Yang Gao [b, 1], Sheng-Hsiang Wang [c], Guey-Rong Sheu [c], Ta-Chih Hsiao [d], Jia-Lin Wang [e], Ming-Cheng Yen [c], Tang-Huang Lin [f], Narisara Thongboonchoo [g], Wei-Chen Chen [c]

[a] Graduate Institute of Energy Engineering, National Central University, Chung-Li, Taiwan
[b] Department of Civil and Environmental Engineering, University of Tennessee, Knoxville, TN, USA
[c] Graduate Institute of Atmospheric Physics, National Central University, Chung-Li, Taiwan
[d] Graduate Institute of Environmental Engineering, National Central University, Chung-Li, Taiwan
[e] Department of Chemistry, National Central University, Chung-Li, Taiwan
[f] Center for Space and Remote Sensing Research, National Central University, Chung-Li, Taiwan
[g] College of Chemical Engineering, King Mongkut's Institute of Technology, Ladkrabang, Bangkok, Thailand

HIGHLIGHTS

- Reanalysis of transport of biomass burning plume originating from SEA.
- Chemical evolution of biomass burning pollutants during long-range transport.
- Combine WRF/HYSPLIT/CMAQ to analyze the compositions of biomass burning plume.

ARTICLE INFO

Article history:
Received 6 November 2014
Received in revised form
20 April 2015
Accepted 24 April 2015
Available online 26 April 2015

Keywords:
Biomass burning
Transport
Chemical evolution
Simulation
2010 Dongsha experiment

ABSTRACT

This study aimed to simulate the transport of biomass burning (BB) aerosol originating from Southeast Asia (SEA) during the Dongsha Experiment conducted from March 2010 to April 2010. Transport pathways were reanalyzed and steering flow in the mid-latitude areas and anticyclones in low-latitude areas were found to control the transport of BB plume after it was injected to a high atmosphere. For the 12 simulated and observed events at Mt. Lulin (2862 m MSL; 23°28′07″ N, 120°52′25″ E), the 72 h backward trajectories were all tracked back to southern China and northern Indochina, which were the locations of the largest BB fire activities in SEA. Chemical evolutions of BB pollutants along the moving trajectories showed that organic matter was always the dominant component in $PM_{2.5}$, consistent with the observations at both near-source regions and Mt. Lulin. For nitrogen species, nearly all NO_x molecules oxidized into HNO_3, NO_3^-, PAN, and PANX in fires or near fires. The synchronic consumption of NO_x, SO_2, and NH_3 explained the production of the major components of inorganic salts. In the moving BB plume, sulfate concentration increased with decreased nitrate concentration. Ratios of ammonium to $PM_{2.5}$ and elemental carbon to $PM_{2.5}$ remained nearly constant because additional sources were lacking.

1. Introduction

Biomass burning (BB) is generally recognized as an important factor that can influence global or regional carbon cycle, meteorology, hydrological cycle, radiative budget, and even climate change. For example, massive amounts of black carbon (BC) in BB aerosols absorb solar radiation and warm the atmosphere of the

* Corresponding author.
E-mail address: mtchuang100@gmail.com (M.-T. Chuang).
[1] Now at: Atmospheric Science and Global Change Division, Pacific Northwest National Laboratory, Richland, Washington, 99352, USA.

http://dx.doi.org/10.1016/j.atmosenv.2015.04.055
1352-2310/

earth (Jacobson, 2001; Gadhavi and Jayaraman, 2010). BB may also cause surface cooling that is related to direct aerosol effects (Sakaeda et al., 2011). Therefore, research on BB pollutants has been gaining attention in recent years. For example, Sciare et al. (2008) observed organic carbon (OC) and BC in Eastern Mediterranean from 2001 to 2006 and found BB aerosols from agricultural wastes burning in European countries around the Black Sea that could travel to Crete Island. Arola et al. (2007) used MODIS satellite data and HYSPLIT model (Draxler and Rolph, 2013) to study the transport of BB aerosols from Eastern Europe to Northern Europe, and the exerted considerable effect on surface radiation. In recent years, the BB around Southeast Asia (SEA) and South Asia was studied. The Seven Southeast Asian Studies (7-SEAS) Mission (http://7-seas.gsfc.nasa.gov/) began in 2010 to study the effect of BB aerosols.

Although Lin et al. (2013), Reid et al. (2013), and other articles published in *Atmospheric Environment* volume 78 and *Atmospheric Research* volume 122 have addressed the properties of BB pollutants in SEA, these references only provide the chemical, physical, optical, and radiative characteristics of BB aerosols and related pollutants in specific sources and downwind locations. Although few studies have used chemical transport models to explain the chemical field of BB pollutants, Fu et al. (2012) applied the CMAQ model to assess the effect of BB aerosols from SEA on East Asia (EA). Their simulations showed that the percentage of effect via long-range transport on downwind regions, including the Pearl River Delta region and Fujian province, could reach 20%–50% on CO, 10%–30% on O_3, and as high as 70% on $PM_{2.5}$. Huang et al. (2013) explained the same event further and suggested that BB in SEA would affect a large area through long-range transport. The contribution of BB to AOD in the downwind regions was significant and ranged from 26% to 62%. However, the chemical evolution of BB aerosol and related chemical species during long-range transport has not been resolved to date.

With regard to the transport of BB pollutants, Lin et al. (2013) implemented the 32-year (1979–2010) monthly mean atmospheric circulation with the National Centers for Environmental Prediction-II reanalysis at 2.5° longitude × 2.5° latitude winds (Kanamitsu et al., 2002) and found that the streamlines that indicated southerly winds at 925 and 850 hPa over Indochina would couple during March and April. The southerly winds climbed over the mountains in northern Indochina and became an upslope wind, which benefits the rise of BB pollutants to approximately 700 hPa. Lin et al. (2009) further suggested that BB pollutants near the surface in Indochina could be driven using the upward transport in the leeside trough on the east side of Tibet Plateau below 3 km and by the horizontal transport in the strong westerly winds prevailing above 3 km. Most of the previous studies focused on the rising mechanism of transporting BB pollutants from the surface to the atmosphere (Lin et al., 2009, 2013; Yen et al., 2013). Recently, Fu et al. (2012) applied the CMAQ model to analyze the transport pathways of BB aerosols from SEA to EA during the 2006 BASE-ASIA campaign (Biomass Burning Aerosols in Southeast Asia: Smoke Impact Assessment) of NASA. Fu et al. (2012) found a slight difference on the effect of BB on the Yangtze River Delta region between March 2006 and April 2006. In March 2006, the effect of BB was mainly concentrated in SEA and southern China. In April 2006, the westerly winds flowing at low latitudes became southwesterly winds that flowed above 15° N, which could push the SEA outflows northward.

In this study, we use data from the 2010 Dongsha experiment (Wang et al., 2011; Lin et al., 2013), which is the preliminary study of the 7-SEAS mission. We first re-analyzed the horizontal transport of BB pollutants from SEA to downwind regions in high altitudes. We then explained the chemical evolution of BB pollutants in BB plume from SEA to Taiwan using two examples. This study provides information about the chemical characteristics of BB plumes, which could further explain optical characteristics and cloud physics for future studies.

2. Methods

2.1. Model description and configuration

The principal modeling tools and resources of the present study are based on those that Fu et al. (2012) and Huang et al. (2013) used. CMAQ model (Byun and Schere, 2006) was used to simulate the chemical field during the 2010 Dongsha experiment from March 2010 to April 2010. The inputs for the CMAQ model included meteorological data from the simulation results of the WRF model (Wang et al., 2012) and various emissions. Anthropogenic emission was based on the 2006 INTEX-B (Intercontinental Chemical Transport Experiment-Phase B) emission inventory of NASA (Zhang et al., 2009). This basis may underestimate the simulated results because the growth of anthropogenic activities from 2006 to 2010 was ignored. Biogenic emissions were generated using the MEGAN (Model of Emission of Gases and Aerosol from Nature) model (Guenther et al., 2012). This model focused on BB emissions from the FLAMBE project (the joint Navy, NASA, NOAA, and Universities Fire Locating and Modeling of Burning Emissions, Reid et al., 2009). Fu et al. (2012) provided further details of model configurations. However, the present study made several changes. For example, the simulation range was changed to three nested domains with resolutions for domains 1, 2, and 3 at 45, 15, and 5 km, respectively (Fig. 1). The simulation results of the second domain were analyzed for chemical evolution along the long-range transport from SEA to Taiwan; the third domain was used for the comparison with the observations at Mt. Lulin in Taiwan. The outputs of the WRF simulation were used for the HYSPLIT model simulation to obtain the historical trajectories of the BB plumes that arrived at Mt. Lulin. From the simulation results, we obtain the BB plumes and chemical compositions at the locations for each hour.

2.2. Uncertainty of BB emissions

Several studies have discussed the uncertainty of BB emissions and indicated the difficult-to-avoid inaccuracies of data, such as burned area, burned time, fuel loading, burning efficiency, and

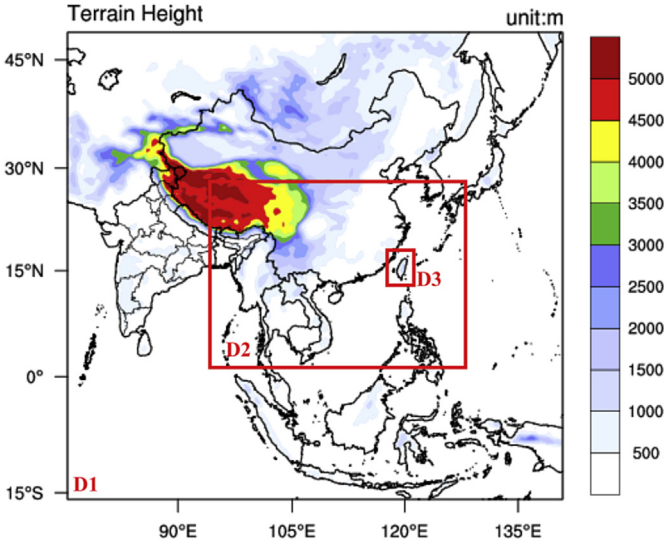

Fig. 1. Three nested domains for current simulation.

burning state, which may lead to uncertainty during emission estimation (Campbell et al., 2007; van der Werf et al., 2006, 2010; French et al., 2011; Zhang et al., 2012). Although several well-known multi-compositions of BB emission inventories exist, which are widely used and readily downloadable (for example, FLAMBE: Reid et al., 2009; GFEDv4: Giglio et al., 2013; IS4FIRES: Soflev et al., 2009. FINN: Wiedinmyer et al., 2011; RCP: van Vuuren et al., 2011), these projects cannot determine the most feasible inventory in all regions around the world or in all periods at all times. The present study followed the previous studies (Fu et al., 2012; Huang et al., 2013) and applied the FLAMBE BB inventory, which also met difficulties. Fu et al. (2012) suggested that CO emission in FLAMBE is probably overestimated in Myanmar and major areas of Thailand, thereby causing an overestimation of CO concentration during peak episodes. They also compared the BB emission inventories for both FLAMBE and GFEDv2 (van der Werf et al., 2006) and found that the former is 7.89 and 11.63 times higher than the latter in March and April 2006 in SEA, respectively. Fu et al. (2012) selected the FLAMBE emission inventory in their study for three reasons. First, the FLAMBE performs better than GFED in terms of simulation with observation at the NASA-owned temporary site in South Thailand. Second, the FLAMBE has an hourly temporal profile. Third, Fu et al. (2012) adopted the suggestion of Nam et al. (2010), in which the GFED emission inventory may underestimate CO at relatively low subtropical latitudes over Asia. Huang et al. (2013) also found the BB emission in the 2006 FLAMBE is overestimated over Myanmar and major areas of Thailand. The criticism about the overestimation of FLAMBE was also suggested in Reid et al. (2009). Therefore, the FLAMBE emission inventory could likely overestimate northern Indochina, which is the main BB source region for downwind areas, including Taiwan.

To increase the quality of quantification of the simulation results, a sensitivity test for the FLAMBE emissions was performed. The BB emission data for all BB emission pollutants were multiplied with 1.0, 0.5, 0.25, 0.125, and 0.0, which were then used as inputs for the simulations. Compared with the continuously monitored CO (Ou-Yang et al., 2014), O_3 (Ou-Yang et al., 2012), and PM_{10} data at Mt. Lulin (Fig. 2) that Taiwan EPA managed, the original BB emission intensity that was multiplied with 0.25 was the most feasible in terms of various statistics, such as RMSE (Root Mean Square Error), MNB (Mean Normalizes Bias), MNE (Mean Normalized Error), MFB (Mean Fractional Bias), MFE (Mean Fractional Error), IOA (Index Of Agreement), F2 (Factor 2 analysis), and R (Correlation Coefficient) (Table 1). Therefore, all BB emissions were reduced by 75% for further analysis. The IOAs of CO, O_3, and PM_{10} are all above 0.6 (Table 1), which indicates a relatively good performance. The purpose of reducing the intensity of BB emissions in the FLAMBE emission inventory was to simulate the scenes and not to tune satisfactory results. However, reducing emission may also compensate for other systematic biases in the modeling system. Compared with the observed concentrations at Mt. Lulin during 7-SEAS/Dongsha Experiment (Lin et al., 2013), the simulated and observed means of $PM_{2.5}$, SO_4^{2-}, NH_4^+, NO_3^-, OC, and EC at Mt. Lulin were 13.7 μg m^{-3} and 14.2 μg m^{-3}, 3.2 μg m^{-3} and 2.3 μg m^{-3}, 1.7 μg m^{-3} and 0.9 μg m^{-3}, 2.4 μg m^{-3} and 0.6 μg m^{-3}, 4.8 μg m^{-3} and 4.6 μg m^{-3}, 0.5 μg m^{-3} and 0.8 μg m^{-3}, respectively. These simulation results agreed well with the observations except for NO_3^-, which were overestimated. As explained later in section 3.2, the condensation of HNO_3 that arose from the drop of temperature when the BB plume approached Mt. Lulin caused the overestimation.

2.3. BB events detected at Mt. Lulin

Given that $PM_{10} > 35$ μg m^{-3} and CO > 0.3 ppm was observed at Mt. Lulin as the standard of events, 12 events were observed and simulated from March 2010 to April 2010 (Fig. 2). These 12 events peaked at Mt. Lulin on March 12, 03:00 h (LST); March 12, 16:00 h; March 16, 18:00 h; March 18, 01:00 h; March 21, 08:00 h; March 25, 17:00 h; March 26, 05:00 h; March 28, 06:00 h; April 5, 19:00 h; April 6, 19:00 h; April 11, 03:00 h; and April 11, 16:00 h. The 72 h backward trajectories starting from Mt. Lulin at the peak hour for

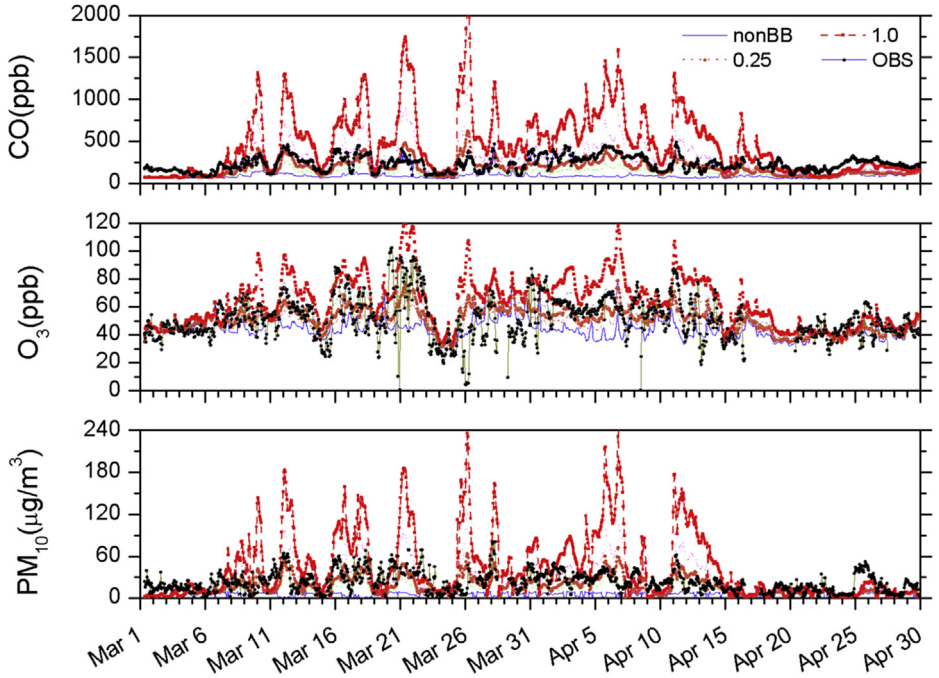

Fig. 2. The comparison of observed and simulated CO, O_3, and PM_{10} at Mt. Lulin site for the BB emission data multiplied with 1.0, 0.25, and 0.0, respectively. Two lines with BB emission data multiplied with 0.5 and 0.125 were skipped but can be imaged to exist between 1.0 and 0.25 and between 0.25 and 0.0.

Table 1
Statistics of sensitivity test for FLAMBE emissions multiplied with different coefficients for observed and simulated CO, O_3, and PM_{10}.

Pollutants	CO					O_3					PM_{10}				
Coefficients	1.0	0.5	0.25	0.125	0.0	1.0	0.5	0.25	0.125	0.0	1.0	0.5	0.25	0.125	0.0
RMSE	398.32	150.84	91.87	117.35	162.66	18.36	12.53	11.83	12.86	15.79	47.96	22.45	16.05	17.12	22.39
MNB	0.95	0.16	−0.22	−0.41	−0.59	0.29	0.14	0.05	0.00	−0.08	1.49	0.48	−0.02	−0.26	−0.57
MNE	1.15	0.48	0.35	0.43	0.59	0.33	0.22	0.20	0.21	0.23	1.95	1.08	0.77	0.70	0.77
MFB	0.39	0.01	−0.32	−0.55	−0.86	0.21	0.10	0.01	−0.04	−0.13	0.14	−0.18	−0.45	−0.65	−1.08
MFE	0.64	0.41	0.42	0.57	0.86	0.25	0.19	0.18	0.20	0.25	0.87	0.76	0.77	0.84	1.17
IOA	0.37	0.66	0.74	0.59	0.45	0.67	0.74	0.67	0.60	0.47	0.39	0.61	0.65	0.56	0.45
F2[0.5,2]	0.54	0.78	0.79	0.61	0.25	0.67	0.98	0.99	0.99	0.98	0.40	0.48	0.50	0.40	0.18
R	0.63	0.64	0.66	0.67	0.38	0.59	0.57	0.52	0.44	0.18	0.43	0.43	0.44	0.45	0.10

Note: the formulas of above statistical parameters RMSE: Root Mean Square Error; MNB: Mean Normalized Bias; MNE: Mean Normalized Gross Error; MFB: Mean Fractional Bias; MFE: Mean Fractional Gross Error, IOA: Index of Agreement; F2: Factor 2; R: Correlation coefficient. The formulas for these statistical parameters can refer to Appendix A in Fu et al., 2012.

the 12 events are illustrated in Fig. 3. As expected, all of the 12 trajectories traced back through southern China/northern South China Sea and to northern/central Indochina because the BB plume that originated from Indochina affected the Mt. Lulin site (Lee et al., 2011; Chuang et al., 2014). Ensemble backward trajectories have also been conducted (not shown), and the 12 trajectories (Fig. 3) have been proven representative. The trajectories between the source region and Taiwan appeared as straight lines, which indicate the shortest path between these two locations (Fig. 3). After the BB plumes were injected into a high altitude, these plumes arrived at Taiwan in approximately 2–2.5 days. This finding implies that the BB plumes arrived in 2–2.5 days and maintained concentrations as high as possible from SEA to Mt. Lin. Although the 12 events were both simulated and observed during the 2010 Dongsha campaign, only two representative events were discussed in the present study. One event occurred in March and the other in April 2010. The rest of the events have similar transport pathways, and the chemical evolution of the BB pollutants to these two events was not repeated.

3. Results and discussion

3.1. Transport pathways of BB plumes

In low-latitude equatorial areas, thermal buoyancy and deep thermal convection, such as the inter-tropical convergence zone (ITCZ) could explain the lifting of BB pollutants (Folkins et al., 1997). However, the thermal convection over Indochina is not as strong as that around the equator and cannot explain the uplifting of BB pollutants. Therefore, other factors help uplift BB pollutants from near the surface to high altitudes, as suggested in previous publications.

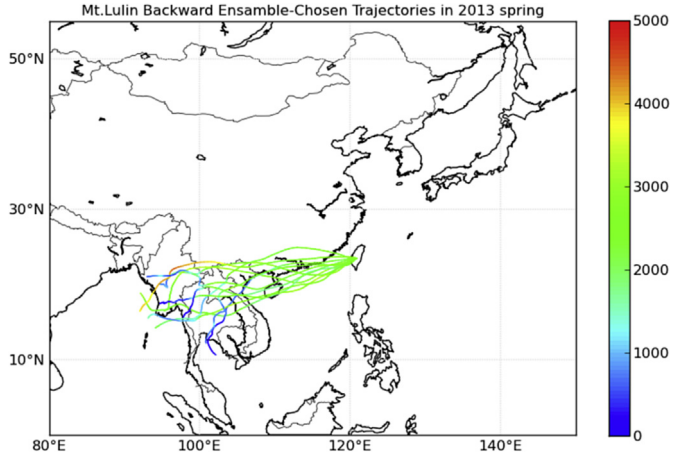

Fig. 3. The 72-h backward trajectories from Mt. Lulin for 12 events in present study.

Several studies have indicated that BB plumes emerging around northern Indochina would ascend to a high atmosphere and then move eastward using the westerly winds (Lin et al., 2009, 2013; Yen et al., 2013). The movement of BB plumes originating from SEA suggests that at least two factors can determine if BB plumes would pass Mt. Lulin. The first factor implies whether forces can help the BB plume rise up above the PBL around the northern/central Indochina. This mechanism includes orographic lifting, the upward motion in low-atmospheric low or a strong updraft in the lee vortex. The second factor implies whether the air stream in the westerly winds can transport the BB plume to Mt. Lulin. Actually, the transport pathways of BB plumes depend on the steering flow in middle-latitude areas and the anticyclone in low-latitude areas over the source and the downwind regions (Fig. 4). Given that the 925 hPa to 700 hPa trough and the BB source region usually overlap over Indochina, the wind fields at the post-trough downwind areas are usually westerly/southwesterly winds. If the BB plumes transport along the southwesterly winds, then the BB plumes may transport northeastward to middle/high-latitude regions. If the wind direction is from the west, then the BB plumes may transport eastward and sometimes transport into the anticyclone in low-latitude areas. For example, on March 15, 2010, most parts of the BB plume followed the steering flow and transported northeastward and only a small part at the south edge was pulled into the anticyclone at low-latitude areas (around two places at 128°E, 20°N and 110°E, 17°N) (Figs. 4a and 5a). Given that the main stream of BB plumes moved northeastward, Taiwan was located at the south edge of the BB plume. When the range of influence from the anticyclone became large, more BB pollutants were transported into the anticyclone (Figs. 4b and 5b). On March 17, 2010, Taiwan was located in the middle of the eastward-moving BB plume. If the range of influence from the anticyclone over the Pacific shrinks (Fig. 4c) and the flow field at the east flank of the trough becomes parallel with line of 30°N, then the BB plume also becomes parallel with 30°N (Fig. 5c). This weather pattern mostly prevents the BB plume from moving to high-latitude areas and only allows movement in low-latitude areas. Therefore, the BB plume may move eastward and pass through south of Taiwan to the Pacific.

In section 2.2, this study has used PM_{10} to validate the model performance. In the following, this study used $PM_{2.5}$ to illustrate the chemical evolution of aerosols in the BB plume. Although $PM_{2.5}$ at Mt. Lulin has no continuous measurement, PM_{10} can be used to replace $PM_{2.5}$ for modeling validation because the $PM_{2.5}/PM_{10}$ ratios were nearly united during BB season (Lin et al., 2013). Furthermore, the simulated mean of $PM_{2.5}$ from March 1 to April 30 2010 was 13.7 $\mu g\ m^{-3}$, which was slightly lower than the measured

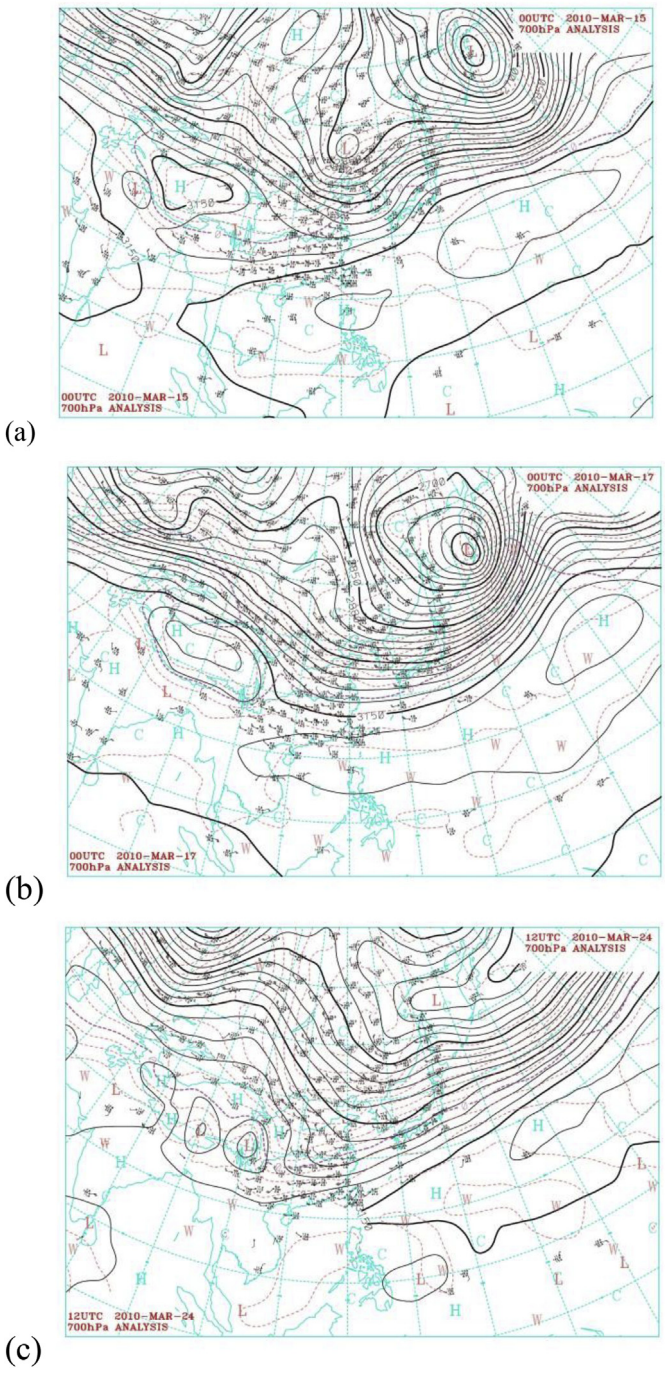

Fig. 4. The 700 hPa weather map at daily 08:00 h on (a) March 15 2010, (b) March 17 2010, and (c) March 25 2010, respectively.

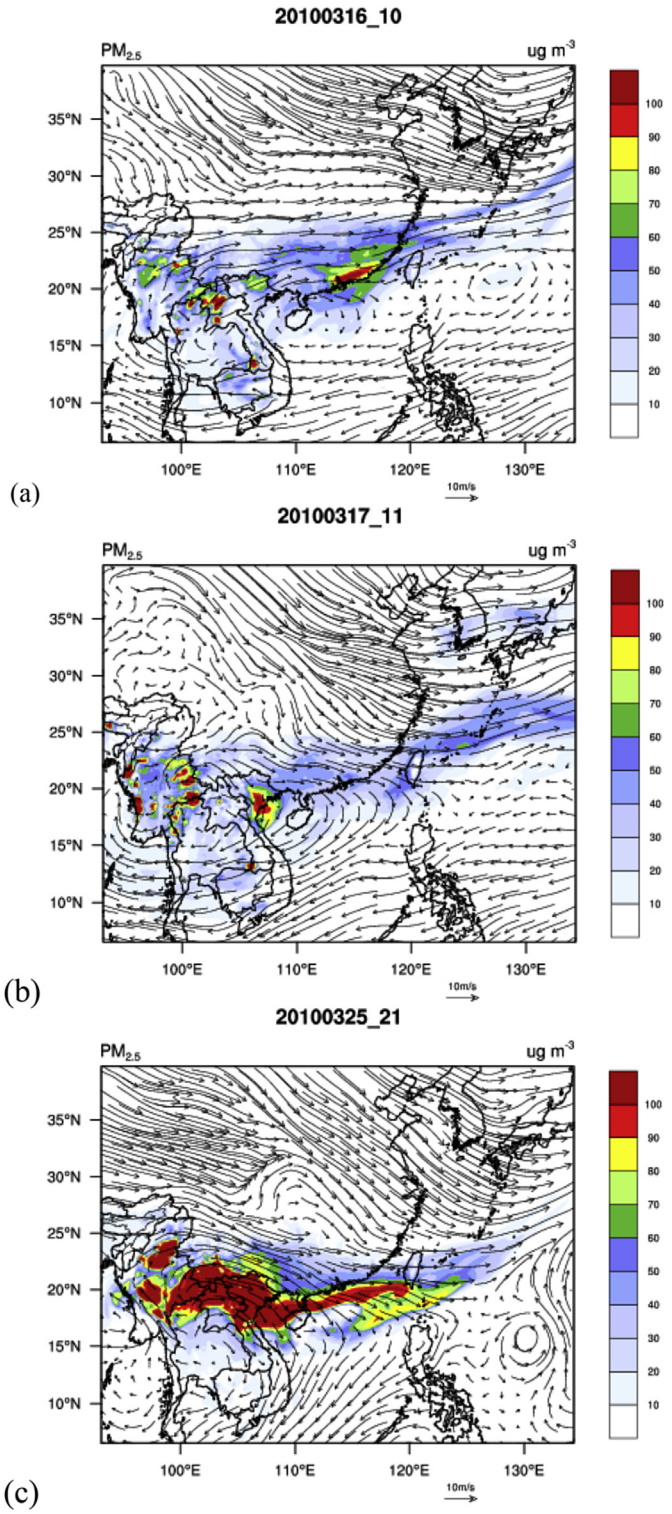

Fig. 5. The simulated $PM_{2.5}$ contour and wind field at layer 10 at (a) 18:00 h March 15 2010, (b) 19:00 h March 17 2010, and (c) 05:00 h March 26 2010, respectively.

mean of $PM_{2.5}$, which was 17.5 μg m^{-3} for the BB events from 2003 to 2009 (Lee et al., 2011). The simulation results should be reasonable because the simulation period also include some non-BB events.

3.2. Chemical evolution of BB pollutants in BB plume

HYSPLIT model was applied to determine the backward trajectory of BB parcel starting from the hour when a peak concentration occurred at Mt. Lulin to the preceding 72 h. Thus, we can understand the chemical evolution of BB pollutants in the BB parcel in the last three days before the BB parcel arrived at Mt. Lulin. However, a peak concentration at Mt. Lulin does not guarantee that the peak concentrations of BB pollutants would always remain at a high level along the backward trajectory because the air near the trajectory can influence the air along the trajectory (i.e., mixing). The air near the trajectory could come from a clean background atmosphere, a new BB plume, an aged BB plume, and a polluted atmosphere from Asia or local pollution. Moreover, the 12 trajectories (Fig. 3) were

similar. However, each event is slightly different from each other because the locations of the emerging BB plume could be different. The BB plumes had different levels of intensity, and the weather conditions also varied. Nevertheless, the air parcel along the trajectory still has most of the characteristics of a BB plume.

3.2.1. BB event on March 12, 2010, 16:00 h

Given that the westerly winds transported the BB plumes horizontally after lifting above the boundary layer, we selected layer 10 among the vertical layers, which has nearest the height of Mt. Lulin (2862 m), to explain the horizontal transport of BB plumes. The $PM_{2.5}$ concentration was approximately 60 μg m^{-3} to 70 μg m^{-3} in the BB parcel (19°N, 120°E) at approximately 3 km aloft and around southern Taiwan on March 10, 2010 (Fig. 6a). At this moment, Taiwan was located north of the BB plume, and the prevailing winds were northwesterly winds. Both the observed PM_{10} (Fig. 2) and simulated $PM_{2.5}$ concentrations at Mt. Lulin were approximately 15 μg m^{-3} to 20 μg m^{-3} because the BB plume did not affect Mt. Lulin. Once the trough became less obvious and the low-latitude anticyclone (14°N to 20°N, 118°E to 135°E) became evident, the northwesterly became westerly winds over the South China Sea (SCS), the local high concentration of BB plume over southern China (20°N, 108°E) moved to SCS, and the foregoing BB plume gradually influenced Mt. Lulin. The observed PM_{10} (Fig. 2) and simulated $PM_{2.5}$ concentrations on March 11, 2010 were approximately 30 μg m^{-3} at Mt. Lulin (Fig. 6b). On March 12, 2010, the westerly winds became southwesterly winds aloft western Taiwan (23°N, 115°E), and part of the concentrated BB plume moved northeastward and passed Mt. Lulin, which observed PM_{10} (Fig. 2) and simulated $PM_{2.5}$ rose to higher than 40 μg m^{-3} (Fig. 6c).

The vertical section A–A (Fig. 6a–c) is indicated in Fig. 7a–c daily at 08:00 h from March 10, 2010 to March 12, 2010. Two intensive fires were located at the mountains of Myanmar (93°E to 95°E) and the border of Myanmar and north of Thailand (97°E to 99°E) below 5 km on March 10, 2010 (Fig. 7a). These two dense plumes were not obvious in layer 10 (Fig. 6a), which was approximately 3 km in height because the $PM_{2.5}$ concentrations reduced rapidly above 3 km. However, an apparent BB plume concentrated at a height of 2.5 km–4 km was located aloft the border of China and Vietnam (104°E to 112°E) (Figs. 6a and 7a). On March 11 at 16:00 h, the BB plume popped out at the border of Myanmar and northern Thailand merged with the downwind plume aloft the border of China and Vietnam, and then moved eastward (Figs. 6b and 7b). On March 12 at 16:00 h, the merged plume ranged from 1.5 km to nearly 5 km vertically and continued to move eastward, which gradually influenced Mt. Lulin (Figs. 6c and 7c). The BB plume continued to move eastward, and the simulated $PM_{2.5}$ concentration at Mt. Lulin increased to above 50 μg m^{-3}. Basically, the simulation result is satisfactorily accepted. The simulated $PM_{2.5}$ at Mt. Lulin was above 30 μg m^{-3} on March 11 at 21:00 h, peaked to 53 μg m^{-3} at on March 12 at 3:00 h, and then decreased below 40 μg m^{-3} until March 12 at 17:00 h. The PM_{10} concentration was above 30 μg m^{-3} since 03:00 h on March 11, peaked to 64 μg m^{-3} at on March 12 at 1:00 h, and then decreased below 40 μg m^{-3} until March 12 at 12:00 h (Fig. 2).

Exploring the chemical evolution of BB pollutants during long-range transport is interesting (16:00 h on March 10, 2010 to 16:00 h on March 12, 2010). The air parcel that originated from Myanmar passed the border of China and Liao and the border of China and Vietnam before arriving at Mt. Lulin. Compared with the distribution of fire figures and emission inventory (not shown), the air parcel can be considered to be part of the BB plume. The BB-related chemical species and their variation in the BB parcel were evaluated for every hour during the aforementioned three-day trajectory. The air parcel that was initialized on March 10 at

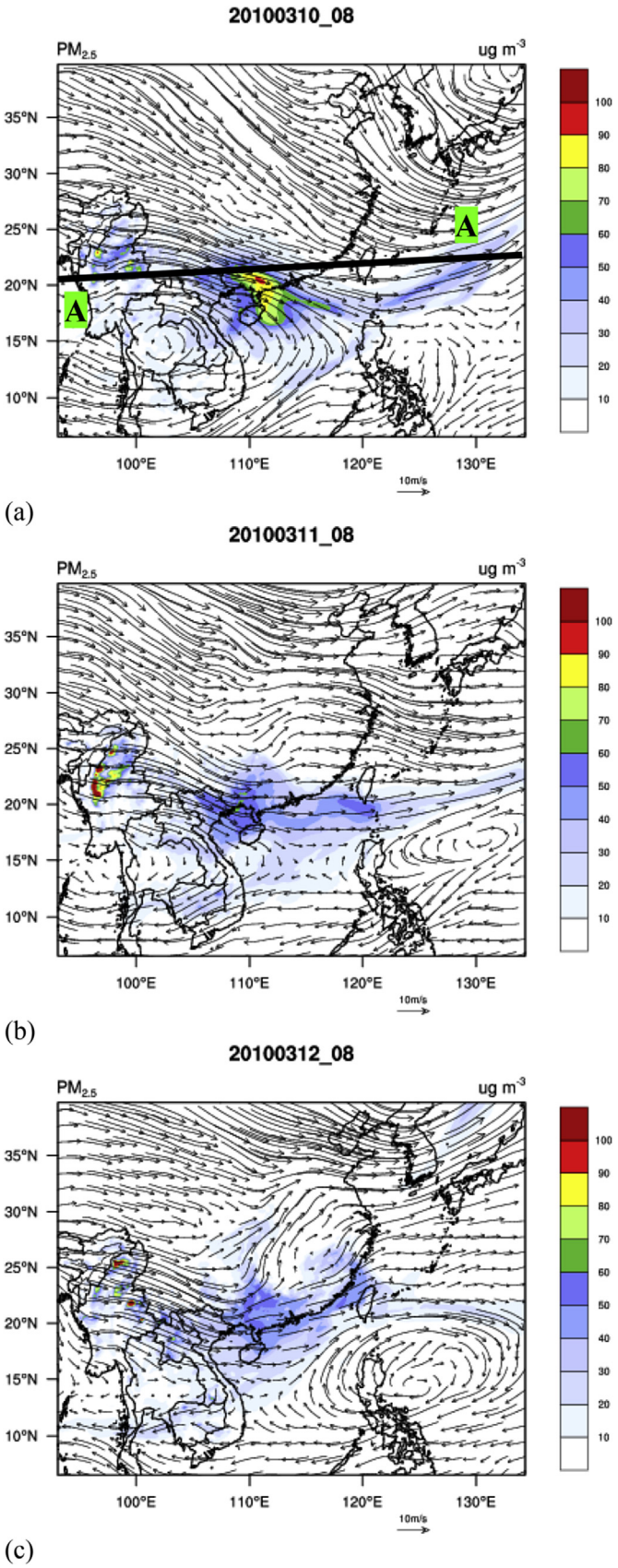

Fig. 6. The simulated $PM_{2.5}$ contour and wind field at layer 10 at daily 16:00 h on (a) March 10 2010, (b) March 11 2010, and (c) March 12 2010, respectively.

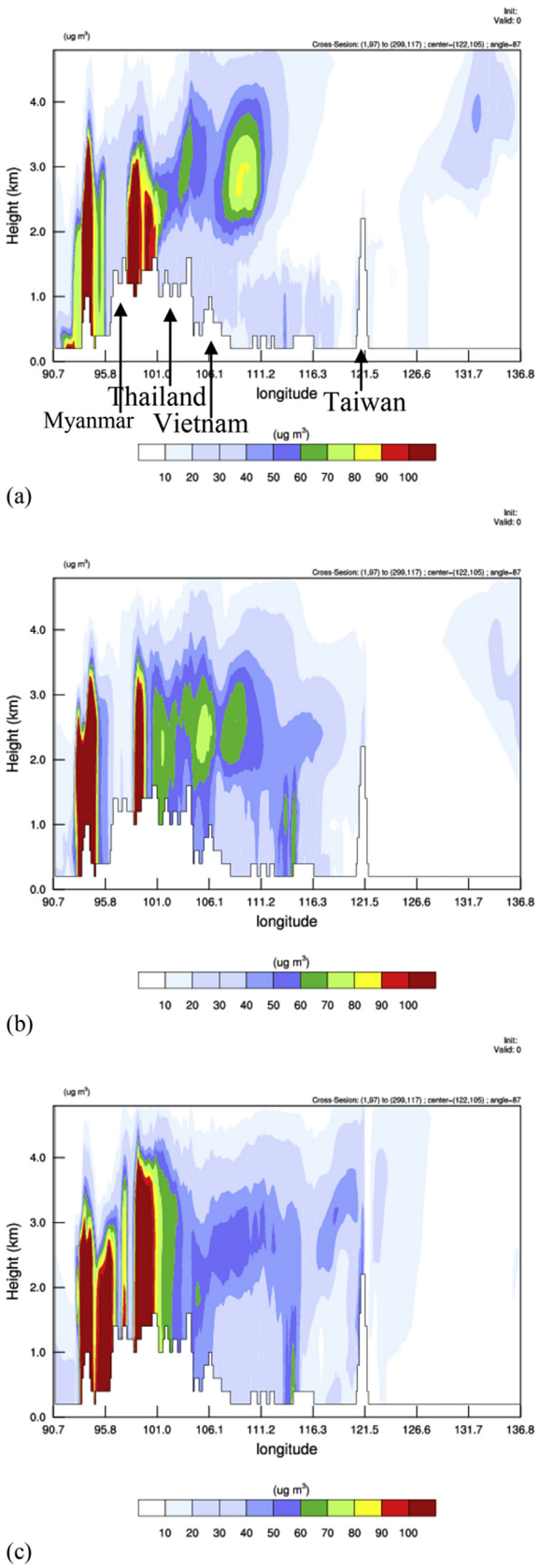

Fig. 7. The simulated $PM_{2.5}$ contour of the vertical section A–A in Fig. 6(a) at daily 16:00 h on (a) March 10 2010, (b) March 11 2010, and (c) March 12 2010, respectively.

16:00 h near surface was soon lifted to approximately 680 hPa (Fig. 8a, approximately 2.5 km height) and mixed with the BB plume that rose from below. During the first 12 h in 3 days, the $PM_{10}/PM_{2.5}$, O_3, and CO were 60 μg m^{-3} to 70 μg m^{-3}, 70 ppb–80 ppb, and 400 ppb–500 ppb, respectively (Fig. 8b). Near the fire source, the nitrogen mainly existed as HNO_3, NH_3, NO_3^-, NH_4^+, peroxyacyl nitrate (PAN), and C3 and high peroxyacyl nitrates (PANX), instead of NO_x. These findings explained that NO_x was converted into secondary forms at the fires or away from the fires. As illustrated in Fig. 9a, the Nitrogen Oxidation Ratio (NOR, ranging from 0.0 to 1.0, the minimum and maximum indicate that nitrogen exists in primary state [NO_2] and secondary state [NO_3^-], respectively; Fan et al., 2015) rapidly increases to over 0.9 at the source regions. The high NOR means that more gas converted into nitrate. The photochemical oxidations have already occurred during plume injection at the source regions. When the air parcel was ready to leave Myanmar, the HNO_3 and NH_3 decreased. By contrast, the proportion of NH_4^+ and NO_3^- in $PM_{2.5}$ began to increase. The nitrogen tended to exist in aerosol phase because the air parcel ascended from the surface to approximately 3 km where the air temperature decreases from 10 °C to −5 °C (Fig. 8c, f, and 8a).

From the position at which the center of the BB parcel was at 02:00 h on March 11 to Mt. Lulin, the O_3, PM_{10}, $PM_{2.5}$, CO, and many chemical species slightly decreased with the distance related to dilution (Fig. 8b). Primary gases, including SO_2, NO_x, and NH_3 decreased to nearly zero because they were converted into the aerosol phase (Fig. 8c and d). The Sulfur Oxidation Ratio (SOR, ranging from 0.0 to 1.0, the minimum and maximum indicates that sulfur exists in the primary state [SO_2] and secondary state [SO_4^{2-}], respectively; Fan et al., 2015) in the BB parcel remained from 0.5 to 0.6 over the source regions and increased to be above 0.6 until the BB parcel moved away from source regions (Fig. 9a). Relatively, the proportion of NO_3^- and NH_4^+ in $PM_{2.5}$ remained nearly constant without affecting dilution with distance (Fig. 8f). On March 12 at 1:00 h, the proportion of NO_3^- in $PM_{2.5}$ decreased but increased again when approaching Mt. Lulin because of condensation. However, the condensation of HNO_3 and formation of NO_3^- could have been overestimated because NO_3^- was overestimated when compared with observations (section 2.2). From Fig. 8a, c, and f, the drop of temperature in the BB plume when approaching Mt. Lulin caused the condensation of HNO_3. By contrast, SO_4^{2-} in $PM_{2.5}$ increased (Fig. 8f). Meanwhile, the SOR increased be nearly 1.0 (Fig. 9a). The air parcel also moved over SCS and descended, and then ambient temperature increased. Part of NH_4NO_3 evaporated, and the evaporated NH_3 reacted with H_2SO_4, which was produced from the conversion of available SO_2 (SO_2 reduced to nearly zero after 01:00 h on March 12 in Fig. 8d). The trend of organic matter (OM) is similar to PM_{10} or $PM_{2.5}$ (Fig. 8e and b) because the proportion of OM in $PM_{2.5}$ was the highest among all aerosol compositions (Fig. 8f). This phenomenon is consistent with observations at both near-sources regions (Chuang et al., 2013) and Mt. Lulin (Chuang et al., 2014). The trend of OM and EC showed that most of the OM was primary OM. In this simulation study, which involves different primary and secondary OMs, the primary OM from the anthropogenic (AORGPAT variable in model outputs) sources were dominant, which accounts for more than 90%. Although primary organic carbon (POC) is more than secondary OC for the SEA BB aerosols sampled at Mt. Lulin (Chuang et al., 2014), the proportion of primary OM from anthropogenic sources could be overestimated in present simulations. This result can be attributed to the possible overestimation of the emission factor of POC in the study by Andreae and Merlet (2001), which is also used in the present study. Robinson et al. (2007) conducted a chamber experiment that revealed substantial evaporation of primary organic aerosol (POA) when very high-temperature emissions are diluted into the

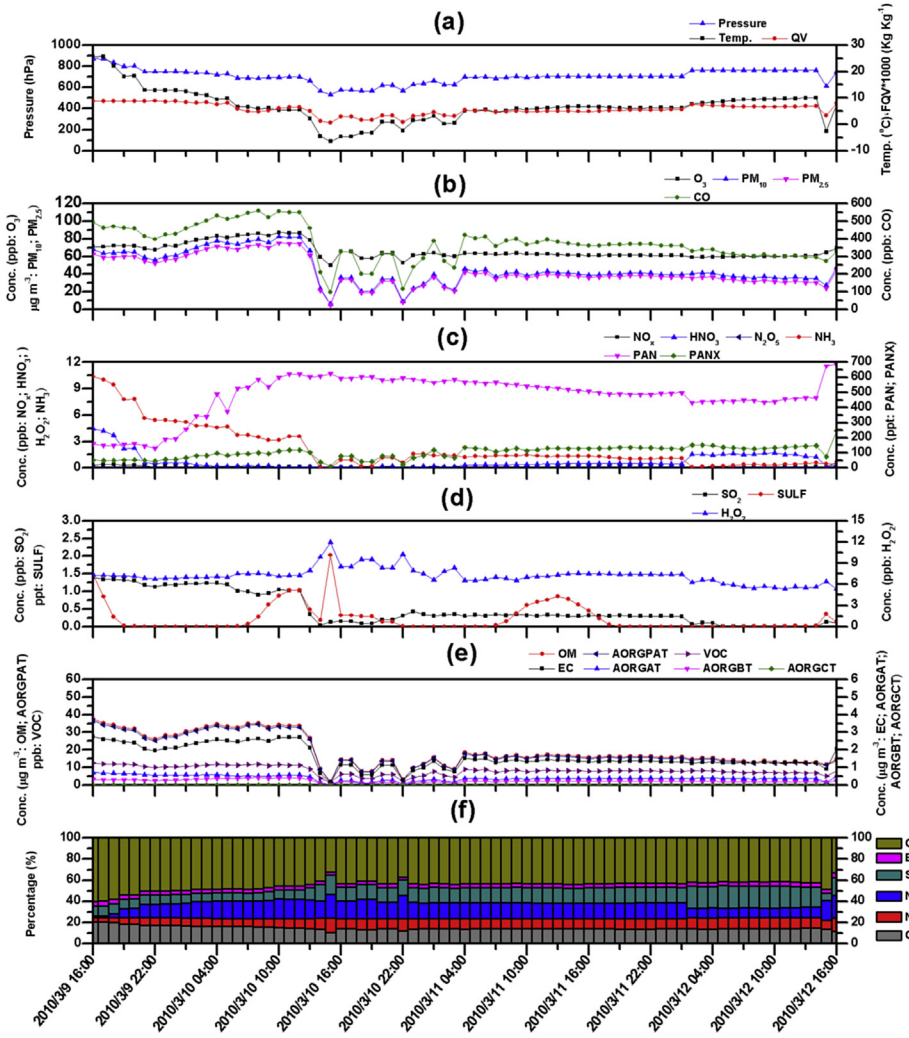

Fig. 8. The chemical evolution of meteorological variables and chemical species in the BB parcel which arrived at Mt. Lulin at 16:00 h on March 12, 2010 (Temp: temperature; QV: water vapor mixing ratio; PAN: peroxy acetyl nitrate; PANX: peroxy propionyl nitrate (PPN) + peroxymethacryloyl nitrate (MPAN); AORGPAT: anthropogenic primary organic aerosol; AORGAT: anthropogenic secondary organic aerosol; AORGBT: biogenic secondary organic aerosol; AORGCT: cloud secondary organic aerosol).

atmosphere. Most of the gaseous volatile organic compounds would condense back to particles after the environment is cooled (Jimenez et al., 2009). In the experiment of Andreae and Merlet (2001), the condensed OM was attributed to the POA. However, the semi-volatile and intermediate-volatility organic compounds that evaporated from POA may form SOA through oxidation from OH attack before condensation. Therefore, the emission factor of POC could be overestimated. By contrast, SOA could be underestimated. For aging aerosols, water-soluble OC (WSOC)/secondary organic aerosol (SOA) is usually produced during long-range transport (Aggarwal and Kawamura, 2009). However, the production of SOA was not obvious in the present simulation. This result

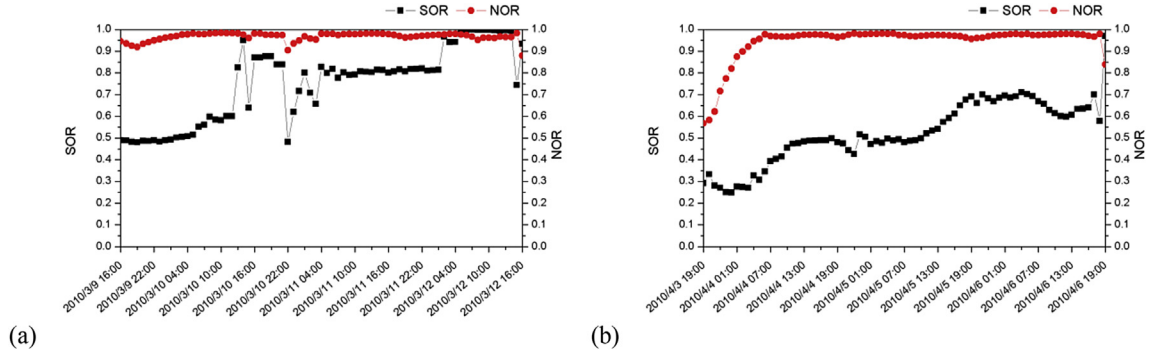

Fig. 9. The variation of sulfur oxidation ratio (SOR) and nitrogen oxidation ratio (NOR) in the BB parcel which arrived at Mt. Lulin (a) at 16:00 h on March 12, 2010 and (b) at 19:00 h on April 6, 2010.

implies that the organic chemistry in CMAQ needs improvement, particularly in the forming SOA. For example, OC may evaporate and oxidize to WSOC and condense on aerosol during long-range transport (Aggarwal and Kawamura, 2009).

3.2.2. BB event on April 6, 2010, 19:00 h

Three days before the occurrence of peak concentration, on April 6, 2010 at 19:00 h, Taiwan was already in the distribution range of the BB plume (Fig. 10a). On April 4, 2010, the simulated $PM_{2.5}$ was approximately between 10 μg m^{-3} and 35 μg m^{-3} at Mt. Lulin (Fig. 10a), which was satisfactory because the observed PM_{10} was between 18 μg m^{-3} and 37 μg m^{-3} (Fig. 2). Although the two high-concentration BB puffs centered over north of Indochina and Hainan, both were still far from Mt. Lulin, and the foregoing BB plume apparently transported eastward and passed Taiwan and the Bashi Channel toward the Pacific. This result is ascribed to the moving direction of the BB plume that was closely connected to the traction of the anticyclone over the SCS, Philippine Sea, and the Pacific Ocean. On April 5, the two large above mentioned BB puffs moved slowly, but only part of the BB puffed over Hainan had rapidly moved to the Bashi Channel (Fig. 10b). This movement caused the overestimation of $PM_{2.5}$ (30 μg m^{-3} to 60 μg m^{-3}) at Mt. Lulin, but the observed PM_{10} was only 20 μg m^{-3} to 45 μg m^{-3}. Part of the BB plume transported to low latitudes because the traction of the anticyclone was obvious on April 6 (Fig. 9c). Similar to the first case discussed in the previous section, the anticyclone in the low latitude served an important function in inhibiting the BB pollutants that spread to high-latitude areas. On April 6, the two BB puffs gradually merged into one elongated BB plume and passed the SCS and the Bashi Channel. Part of the BB pollutants passed Taiwan and moved northeastward, and another part continued to flow into the anticyclone. The overestimated simulated $PM_{2.5}$ and observed PM_{10} were 30 μg m^{-3} to 70 μg m^{-3} (Fig. 10c) and 20 μg m^{-3} to 40 μg m^{-3}, respectively. Although the $PM_{2.5}$ concentration at Mt. Lulin was overestimated, the trends of the simulated $PM_{2.5}$ and observed PM_{10} were similar (Fig. 2).

The vertical sections A–A (Fig. 10a–c) are indicated in Fig. 11a–c at 19:00 h daily from April 4, 2010 to April 6, 2010. On April 4, the BB plume originated from the mountains in northern Vietnam (Fig. 11a). However, the intensity of the BB plume is not as strong as those originating from the mountains in Myanmar and in the border of Myanmar and north of Thailand (Fig. 11c, Fig. 7a–c). Therefore, the BB plume did not eject vertically but rose and moved eastward simultaneously (Fig. 11b, BB puff centered at 112°E, 2 km). On April 5, the foregoing BB plume continued to influence Mt. Lulin and decelerated because the anticyclone caused the BB plume to change direction (Fig. 11b). On April 6, the leading edge of the above mentioned BB puff centered at 112°E, 2 km further and covered the whole of Taiwan (Fig. 11c, BB puff centered at 120°E, 2.5 km).

On April 3, 2010, the BB parcel was aloft northern Laos and northern Vietnam, and the $PM_{2.5}$ concentration in the parcel could reach 200 μg m^{-3} (Fig. 12b). After the BB parcel moved away from the BB sources, the air parcel began to descend, and the ambient atmospheric pressure and ambient temperature gradually increased (Fig. 12a). All of the concentrations of major BB pollutants decreased because of the dilution with the transport distance (Fig. 12b). After the BB parcel moved away from the fire sources, NO_x in the air parcel was consumed, and PAN, PANX, and HNO_3 were produced instead (Fig. 12c). As illustrated in Fig. 9b, the NOR increased to be over 0.5 at the source regions. The NOR at the source regions is lower than that (above 0.9) for the March 12 event because the NO_x concentration was high for this event. However, the NOR still increased to be above 0.9 soon after the BB parcel was away from the source regions (Fig. 9b). The SO_2 concentration in

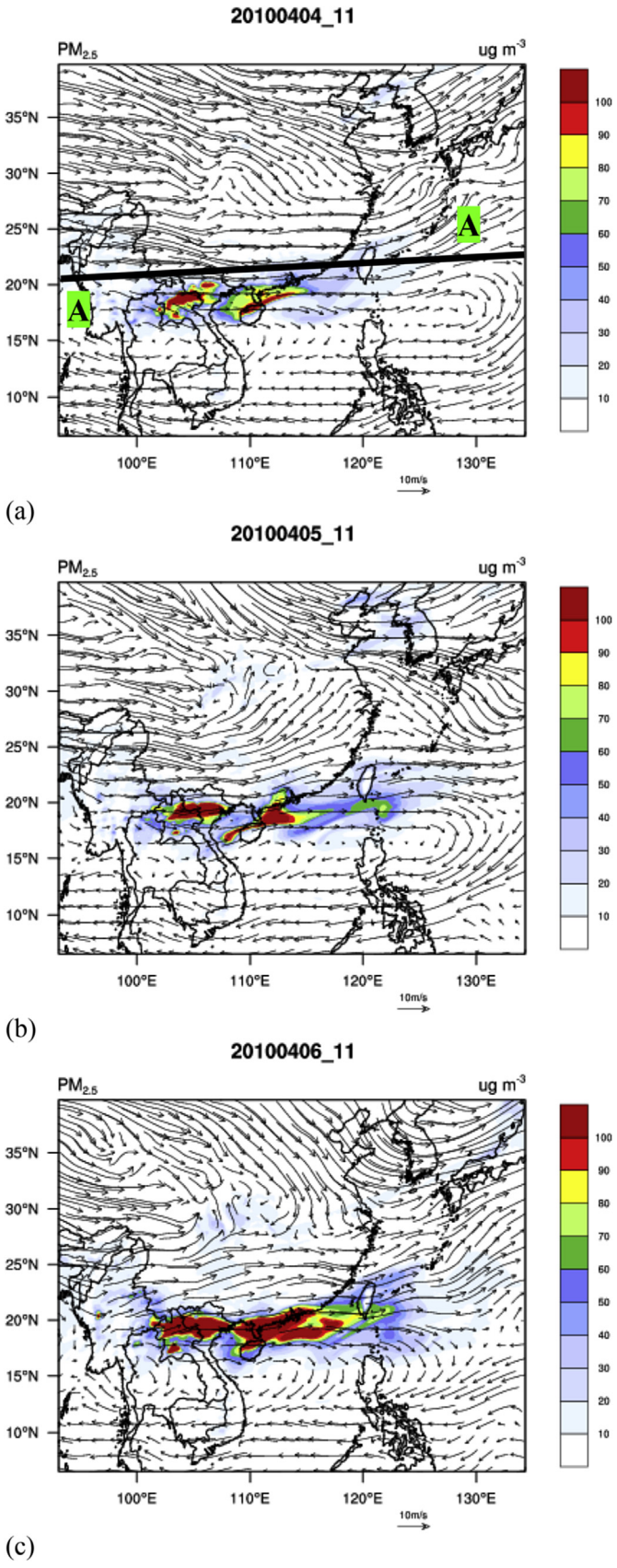

Fig. 10. The simulated $PM_{2.5}$ contour and wind field at layer 10 at daily 19:00 h on (a) April 4 2010, (b) April 5 2010, and (c) April 6 2010, respectively.

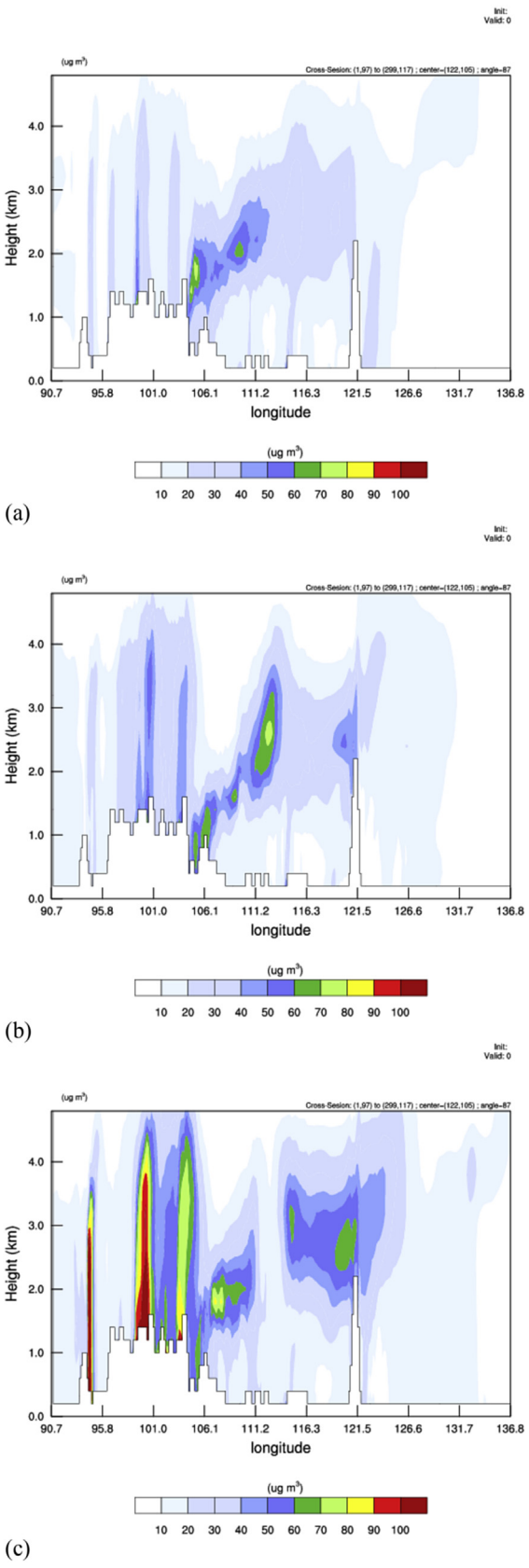

Fig. 11. The simulated $PM_{2.5}$ contour of the vertical section A–A in Fig. 10(a) at daily 19:00 h on (a) April 4 2010, (b) April 5 2010, (c) April 6 2010, respectively.

this event was also higher than that in the March 12 event (Fig. 12d). The SOR was relatively lower than the source regions, which is approximately 0.3 (Fig. 9b). On April 4 at 23:00 h, the BB parcel that moved eastward over Hainan suddenly fell approximately 500 m, and the ambient temperature increased to approximately 5 °C. This movement decreased the amounts of NO_3^- and NH_4^+ to 8.8 μg m^{-3} and 3.8 μg m^{-3}, respectively. HNO_3 and NH_3 also increased to approximately 2.2 ppb and 0.9 ppb, respectively. On April 5, the trends of NH_3 and HNO_3 were almost the same. The NO_3^- and NH_4^+ in $PM_{2.5}$ exhibited an opposite trend (Fig. 12f). The PAN continuously decreased during the transport because of the dilution and conversion to the aerosol phase. Meanwhile, SO_2 concentrations continuously decreased because of oxidation and diffusion (Fig. 12d). Relatively, the percentage of SO_4^{2-} in $PM_{2.5}$ gradually increased (Fig. 12f). Hereafter, the BB parcel moved northeastward and continued to mix with clean air from the SCS. The concentrations of major BB pollutants, such as PM_{10}/$PM_{2.5}$, OM, EC, and CO, gradually decreased until approximately 12 h before reaching Mt. Lulin (Fig. 12b and e). Most of the BB pollutants were enhanced when the BB plume approached Mt. Lulin. The moving air that was blocked and squeezed in the windward side of the Central Mountain Range did not influence the enhancement. Instead, pollutants from Asia influenced the enhancement. This result implied that SO_2 was also enhanced but was negligible in fresh BB plume. Once the SO_2 in the fresh BB plume was consumed, its concentration should remain at approximately zero. During the long-range transport, the variation of SULF is in wave form because SULF was mainly produced through gas-phase reaction of SO_2 and OH, which usually dominates at noon (Stockwell and Calvert, 1983). In this case, the aqueous-phase reaction for the production of SULF was insignificant because the peak of H_2O_2 was behind the peak of SULF (Fig. 12a), and the water mixing ratio remained constantly low (Fig. 12a) (Kleinman, 1991). Since the second day, the trends of SO_2 and H_2O_2 were nearly the same. This finding indicates that the BB parcel was not found in the environment-like clouds or fogs (Pandis and Seinfeld, 1989). Similar to the March 12 event, the proportion of OM in $PM_{2.5}$ was the highest among all aerosol compositions (Fig. 12f). Meanwhile, the trend of EC, the anthropogenic POA, and OM were similar (Fig. 12e). This result implies that the primary OM could be overestimated and relatively, the SOA is underestimated. Therefore, the evaporation of VOCs from POA and the oxidation and condensation of oxidized VOCs to form SOA were eager to be discovered and incorporated into art-air quality models.

If the bottom of the plume is below the heights of the mountains in Taiwan, then the air quality on the approaching BB plumes could influence the air quality on the ground. Yen et al. (2013) explained that the downward airstream along with the passage of the front could bring high-elevation BB plume to the ground. An explanation to this situation is worth studying. In addition, the chemical reactions of BB pollutants and the locally emitted pollutants should produce few secondary products because the precursor gas concentrations in the BB plumes of the above mentioned events were low when approaching Taiwan. This hypothesis must be verified and the detailed discussion of the BB plume approaching Taiwan will be discussed in the near future.

4. Conclusions

This study is part of the 2010 Dongsha Experiment and a pre-study of the 7-SEAS project. The WRF and CMAQ modeling system was used to simulate the transport and chemical evolution of BB plume from source regions to the Mt. Lulin site in Taiwan.

Our simulation results reanalyzed the transport of BB plumes and found that after the BB pollutants were injected to high

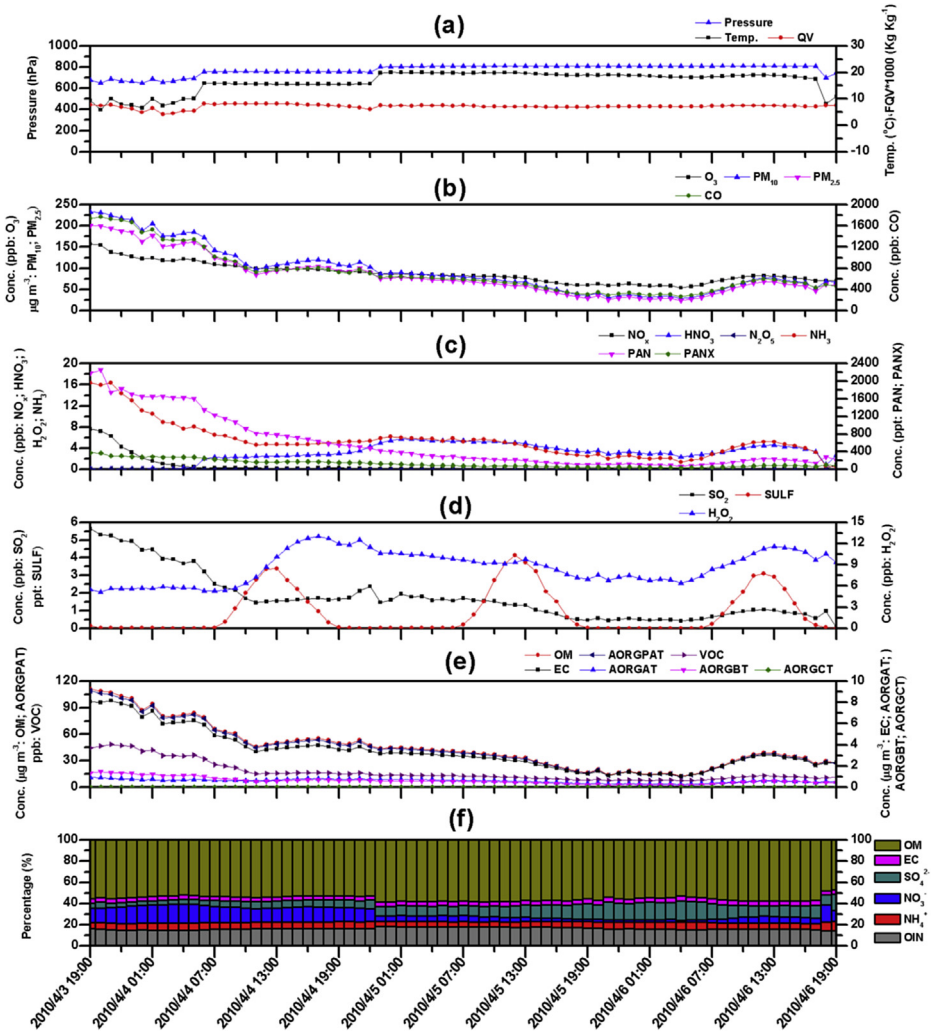

Fig. 12. The chemical evolution of meteorological variables and chemical species in the BB parcel which arrived Mt. Lulin at 19:00 h on April 6, 2010 (Temp: temperature; QV: water vapor mixing ratio; PAN: peroxy acetyl nitrate; PANX: peroxy propionyl nitrate (PPN) + peroxymethacryloyl nitrate (MPAN); AORGPAT: anthropogenic primary organic aerosol; AORGAT: anthropogenic secondary organic aerosol; AORGBT: biogenic secondary organic aerosol; AORGCT: cloud secondary organic aerosol).

altitudes, the steering flow in middle latitude areas and anticyclone in low-latitude areas controlled the transport of BB plumes. If the BB plumes were transported along the southwesterly winds, then the BB plumes may transport northeastward to the middle/high-latitude regions. If the BB plume transported along the westerly winds, then the BB plumes may transport eastward and sometimes transport into the anticyclone. Therefore, Taiwan could be located north, south or in the middle of the BB plume. Two events of BB plume transport were addressed. Both events showed that OM accounted for the highest proportion in $PM_{2.5}$ among all of the species. The proportion of EC in $PM_{2.5}$ and NH_4^+ in $PM_{2.5}$ increased near the fire source and then remained nearly constant during transport. Even when the BB parcel was near fire sources, NO_x was converted into HNO_3, NO_3^-, PAN, and PANX. Along the long range transport, nitrate decreased and relatively sulfate increased. Meanwhile, air from Asia also influenced SO_4^{2-}.

On the other hand, since the carbonaceous content dominates the BB aerosols, the organic chemistry in air quality models like CMAQ is needed to be improved in order to illustrate the SOA production. In addition, the FLAMBE BB emission inventory was reduced by a factor of 4 in current study. The sensitivity test suggested the deviation of emission inventory should be resolved for future studies.

Acknowledgments

We express our deep gratitude for the support from the Taiwan National Science Council under grants NSC 100-2111-M-008-017-, NSC 101-2111-M-008-005-, and NSC 102-2111-M-008-010-. We also thank the Taiwan Environmental Protection Agency for the data retrieval at LABS. We acknowledge the US NCEP for providing us with FNL data, as well as the Data Bank of Atmospheric Research managed by the National Taiwan University for the meteorological maps.

References

Aggarwal, S.G., Kawamura, K., 2009. Carbonaceous and inorganic composition in long-range transported aerosols over northern Japan: implication for aging of water-soluble organic fraction. Atmos. Environ. 43, 2532–2540.
Andreae, M.O., Merlet, P., 2001. Emission of trace gases and aerosols from biomass burning. Glob. Biogeochem. Cycles 15, 955–966.
Arola, A., Lindfors, A., Natunen, A., Lehtinen, K.E.J., 2007. A case study on biomass burning aerosols: effects on optical properties and surface radiation levels. Atmos. Chem. Phys. 7, 4257–4266.
Byun, D., Schere, K.L., 2006. Review of the governing equations, computational algorithms, and other components of the models-3 community multiscale air quality (CMAQ) modeling system. Appl. Mech. Rev. 59, 51–77.
Campbell, J., Donato, D., Azuma, D., Law, B., 2007. Pyrogenic carbon emission from a large wildfire in Oregon, United States. J. Geophys. Res. 112, G04014. http://

dx.doi.org/10.1029/2007JG000451.
Chuang, M.T., Chou, C.K., Sopajareepom, K., Lin, N.H., Wang, J.L., Sheu, G.R., Chang, Y.C., Lee, C.T., 2013. Characterization of aerosol chemical properties from near-source biomass burning in Chiang Mai, Thailand during 7-SEAS/Dongsha experiment. Atmos. Environ. 78, 72–81.
Chuang, M.T., Lee, C.T., Lin, N.H., Chou, C.C.K., Wang, J.L., Sheu, G.R., Chang, S.C., Wang, S.H., Huang, H., Cheng, H.W., Weng, G.H., Lai, S.Y., Hsu, S.P., Chang, Y.J., 2014. Carbonaceous aerosols in the biosmoke transported from Indochina to Taiwan: long-term observation at Mountain Lulin. Atmos. Environ. 89, 507–516.
Draxler, R.R., Rolph, G.D., 2013. HYSPLIT (HYbrid Single-particle Lagrangian Integrated Trajectory) Model Access via NOAA ARL READY. NOAA Air Resources Laboratory, College Park, MD.. http://www.arl.noaa.gov/HYSPLIT.php
Fan, Q., Lan, J., Liu, Y., Wang, X., Chau, P., Fan, S., Hong, Y., Liu, Y., Zeng, Y., Liang, G., Feng, Y., 2015. Diagnostic analysis of the sulfate aerosol pollution in spring over Peal River Delta, China. Aerosol Air Qual. Res. 15, 46–57. http://dx.doi.org/10.4209/aaqr.2014.03.004.
Folkins, A.R., Chatfield, D., Baumgardner, D., Proffitt, D., 1997. Biomass burning and deep convection in southeastern Asia: results from ASHOE/MAESA. J. Geophys. Res. 102, 13291–13299.
French, N.H.F., de Groot, W.J., Jenkins, L.K., Rogers, B.M., Alvarado, E., Amiro, B., de Jong, B., Goetz, S., Hoy, E., Hyer, E., Keane, R., Law, B.E., McKenzie, D., McNulty, S.G., Ottmar, R., Pérez-Salicrup, D.R., Randerson, J., Robertson, K.M., Turetsky, M., 2011. Model comparisons for estimating carbon emissions from North American wildland fire. J. Geophys. Res. 116, G00K05. http://dx.doi.org/10.1029/2010JG001469.
Fu, J.S., Hsu, N.C., Gao, Y., Huang, K., Li, C., Lin, N.-H., Tsay, S.-C., 2012. Evaluating the influence of biomass burning during 2016 BASE-ASIA: a regional chemical transport modeling. Atmos. Chem. Phys. 12, 3837–3855.
Gadhavi, H., Jayaraman, A., 2010. Absorbing aerosols: contribution of biomass burning and implications for radiative forcing. Ann. Geophys. 28, 103–111.
Giglio, L., Randerson, J.T., van der Werf, G.R., 2013. Analysis of daily, monthly, and annual burned area using the fourth-generation global fire emissions database (GFED4). J. Geophys. Res. Biogeosciences 118, 317–328.
Guenther, A.B., Jiang, X., Heald, C.L., Sakulyanontvittaya, T., Duhl, T., Emmons, L.K., Wang, X., 2012. The model of emissions of gases and aerosols from nature version 2.1 (MEGAN2.1): an extended and updated framework for modeling biogenic emissions. Geosci. Model Dev. 5, 1471–1492.
Huang, K., Fu, J.S., Hsu, N.C., Gao, Y., Dong, X., Tsay, S.-C., Lam, Y.F., 2013. Impact assessment of biomass burning on air quality in Southeast and East Asia during BASE-ASIA. Atmos. Environ. 78, 291–302.
Jacobson, M.Z., 2001. Strong radiative heating due to the mixing state of black carbon in atmospheric aerosols. Nature 409, 695–697.
Jimenez, J.L., Canagaratna, M.R., Donahue, N.M., Prevot, A.S.H., Zhang, Q., Kroll, J.H., DeCarlo, P.F., Allan, J.D., Coe, H., Ng, N.L., Aiken, A.C., Docherty, K.S., Ulbrich, I.M., Grieshop, A.P., Robinson, A.L., Duplissy, J., Smith, J.D., Wilson, K.R., Lanz, V.A., Hueglin, C., Sun, Y.L., Tian, J., Laaksonen, A., Raatikainen, T., Rautiainen, J., Vaattovaara, P., Ehn, M., Kulmala, M., Tomlinson, J.M., Collins, D.R., Cubison, M.J., Dunlea, E.J., Huffman, J.A., Onasch, T.B., Alfarra, M.R., Williams, P.I., Bower, K., Kondo, Y., Schneider, J., Drewnick, F., Borrmann, S., Weimer, S., Demerjian, K., Salcedo, D., Cottrell, L., Griffin, R., Takami, A., Miyoshi, T., Hatakeyama, S., Shimono, A., Sun, J.Y., Zhang, Y.M., Dzepina, K., Kimmel, J.R., Sueper, D., Jayne, J.T., Herndon, S.C., Trimborn, A.M., Williams, L.R., Wood, E.C., Middlebrook, A.M., Kolb, C.E., Baltensperger, U., Worsnop, D.R., 2009. Evolution of organic aerosols in the atmosphere. Science 326, 1525–1529.
Kanamitsu, M., Ebisuzaki, W., Woollen, J., Yang, S.-K., Hnilo, J.J., Fiorino, M., Potter, G.L., 2002. NCEP-DEO AMIP-II reanalysis (R-2). Bull. Am. Meteorological Soc. 83, 1631–1643.
Kleinman, L.I., 1991. Seasonal dependence of boundary layer peroxide concentration: the low and high NOx regimes. J. Geophys. Res. 96, 20721–20733.
Lee, C.T., Chuang, M.T., Lin, N.H., Wang, J.L., Sheu, G.R., Wang, S.H., Huang, H., Chen, H.W., Weng, G.H., Hsu, S.P., 2011. The enhancement of biosmoke from Southeast Asia on $PM_{2.5}$ water-soluble ions during the transport over the Mountain Lulin site in Taiwan. Atmos. Environ. 45, 5784–5794.
Lin, C.-Y., Hsu, H.-m., Lee, Y.H., Kuo, C.H., Sheng, Y.-F., Chu, D.A., 2009. A new transport mechanism of biomass burning from Indochina as identified by modeling studies. Atmos. Chem. Phys. 9, 7901–7911. http://dx.doi.org/10.5194/acp-9-7901-2009.
Lin, N.H., Tsay, S.C., Reid, J.S., Yen, M.C., Sheu, G.R., Wang, S.H., Chi, K.H., Chuang, M.T., Ou-Yang, C.F., Fu, J.S., Lee, C.T., Wang, L.C., Wang, J.L., Hsu, C.N., Holben, B.N., Chu, Y.C., Maring, H., Anh, X.N., Sopajaree, K., Chen, S.J., Cheng, M.T., Tsuang, B.J., Tsai, C.J., Peng, C.M., Chang, C.T., Lin, K.S., Tsai, Y.I., Lee, W.J., Chang, S.C., Liu, J.J., Chiang, W.L., 2013. An overview of regional experiments on biomass burning aerosols and related pollutants in Southeast Asia: from BASE-ASIA and Dongsha experiment to 7-SEA. Atmos. Environ. 78, 1–19.
Nam, J., Wang, Y., Luo, C., Chu, D.A., 2010. Trans-Pacific transport of Asian dust and CO: accumulation of biomass burning CO in the subtropics and dipole structure of structure. Atmos. Chem. Phys. 10, 3297–3308.
Ou-Yang, C.F., Lin, N.H., Sheu, G.R., Lee, C.T., Wang, J.L., 2012. Seasonal and diurnal variations of ozone at a high-altitude mountain baseline station in East Asia. Atmos. Environ. 46, 279–288. http://dx.doi.org/10.1016/j.atmosenv.2011.09.060.
Ou-Yang, C.F., Lin, N.H., Lin, C.C., Wang, S.H., Sheu, G.R., Lee, C.T., Schnell, R.C., Lang, P.M., Kawasato, T., Wang, J.L., 2014. Characteristics of atmospheric carbon monoxide at a high-mountain background station in East Asia. Atmos. Environ. 89, 613–622.
Pandis, S.N., Seinfeld, J.H., 1989. Mathematical modelling of acid deposition due to radiation fog. J. Geophys. Res. 94, 12911–12923.
Reid, J.S., Hyer, E.J., Prins, E.M., Westphal, D.L., Zhang, J., Wang, J., Christopher, S.A., Curtis, C.A., Schmidt, C.C., Eleuterio, D.P., Richardson, K.A., Hoffman, J.P., 2009. Global monitoring and forecasting of biomass-burning smoke: description of and lessons from the fire locating and modeling of burning emissions (FLAMBE) program, selected topics in applied earth observations and remote sensing. IEEE J. Sel. Top. Appl. Earth Observations Remote Sens. 2, 144–162.
Reid, J.S., Hyer, E.J., Johnson, R.S., Holben, B.N., Yokelson, R.J., Zhang, J., Campbell, J.R., Christopher, S.A., Girolamo, L.D., Giglio, L., Holz, R.E., Kearney, C., Miettinen, J., Reid, E.A., Turk, F.J., Wang, J., Xian, P., Zhao, G., Balasubramanian, R., Chew, B.N., Janai, S., Lagrosas, N., Lestari, P., Lin, N.-H., Mahmud, M., Nguyen, A.X., Norris, B., Oahn, N.T.K., Oo, M., Salinas, S.V., Welton, E.J., Liew, S.C., 2013. Observing and understanding the Southeast Asian aerosol system by remote sensing: an initial review and analysis for the Seven Southeast Asian studies (7SEAS) program. Atmos. Res. 103 http://dx.doi.org/10.1016/j.atmosres.2012.06.005.
Robinson, A.L., Donahue, N.M., Shrivastava, M.K., Weitkamp, E.A., Sage, A.M., Grieshop, A.P., Lane, T.E., Pierce, J.R., Pandis, S.N., 2007. Rethinking organic aerosols: semivolatile emissions and photochemical aging. Science 315, 1259–1262.
Sakaeda, N., Wood, R., Rasch, P.J., 2011. Direct and semidirect aerosol effects of southern African biomass burning aerosol. J. Geophys. Res. 116, D12205. http://dx.doi.org/10.1029/2010JD015540.
Sciare, J., Oikonomou, K., Favez, O., Liakakou, E., Markaki, Z., Cachier, H., Mihalopoulos, N., 2008. Long-term measurements of carbonaceous aerosols in the Eastern Mediterranean: evidence of long-range transport of biomass burning. Atmos. Chem. Phys. 8, 5551–5563.
Sofiev, M., Vankevich, R., Lotjonen, M., Prank, M., Petukhov, V., Ermakova, T., Koskinen, J., Kukkonen, J., 2009. An operational system for the assimilation of the satellite information on wild-land fires for the needs of air quality modelling and forecasting. Atmos. Chem. Phys. 9, 6833–6847. http://dx.doi.org/10.5194/acp-9-6833-2009.
Stockwell, W.T., Calvert, J.G., 1983. The mechanism of the HO-SO_2 reaction. Atmos. Environ. 17, 2231–2235.
van der Werf, G.R., Randerson, J.T., Giglio, L., Collatz, G.J., Kasibhatla, P.S., Arelano Jr, A.F., 2006. Interannual variability in global biomass burning emissions from 1997 to 2004. Atmos. Chem. Phys. 6, 3423–3441.
van der Werf, G.R., Randerson, J.T., Giglio, L., Collatz, G.J., Mu, M., Kasibhatla, P.S., Morton, D.C., DeFries, R.S., Jin, Y., van Leeuwen, T.T., 2010. Global fire emissions and the contribution of deforestation, savanna, forest, agricultural, and peat fires (1997–2009). Atmos. Chem. Phys. 10, 16153–16230. http://dx.doi.org/10.5194/acpd-10-16153-2010.
van Vuuren, D.P., Edmonds, J., Kainuma, M., Riahi, K., Thomson, A., Hibbard, K., Hurtt, G.C., Kram, T., Krey, V., Lamarque, J.F., Masui, T., Meinshausen, M., Nakicenovic, N., Smith, S.J., Rose, S.K., 2011. The representative concentration pathways: an overview. Clim. Change 109, 5–31.
Wang, S.-H., Tsay, S.-C., Lin, N.-H., Hsu, N.C., Bell, S.W., Li, C., Ji, Q., Jeong, M.-J., Hansell, R.A., Welton, E.J., Holben, B.N., Sheu, G.-R., Chu, Y.-C., Chang, S.-C., Liu, J.-J., Chiang, W.-L., 2011. First detailed observations of long-range transported dust over the northern South China Sea. Atmos. Environ. 45, 4404–4448. http://dx.doi.org/10.1016/j.atmosenv.2011.04.077.
Wang, W., Bruyère, C., Duda, M., Dudhia, J., Gill, L., Lin, H.C., Michalakes, J., Rizvi, S., Zhang, X., Beezley, J.D., Coen, J.I., Mandel, J., 2012. ARW version 3 modeling system user's guide. Mesoscale & Miscroscale Meteorology Division, National Center for Atmospheric Research. July 2010, last updated January 2012.
Wiedinmyer, C., Akagi, S.K., Yokelson, R.J., Emmons, L.K., Al-Saadi, J.A., Oriando, J.J., Soja, A.J., 2011. The fire Inventory from NCAR (FINN): a high resolution global model to estimate the emissions from open burning. Goescientific Model Dev. 4, 625–641.
Yen, M.C., Peng, C.M., Chen, T.C., Chen, C.S., Lin, N.H., Tzeng, R.Y., Lee, Y.A., Lin, C.C., 2013. Climate and weather characteristics in association with the active fires in northern Southeast Asia and spring air pollution in Taiwan during 2010 7-SEAS/Dongsha experiment. Atmos. Environ. 78, 35–90.
Zhang, Q., Streets, D.G., Carmichael, G.R., He, K.B., Huo, H., Kannari, A., Klimont, Z., Park, I.S., Reddy, S., Fu, J.S., Chen, D., Duan, L., Lei, Y., Wang, L.T., Yao, Z.I., 2009. Asian emissions in 2006 for the NASA INTEX-B missions. Atmos. Chem. Phys. 9, 5131–5153.
Zhang, X., Kondragunta, S., Ram, J., Schmidt, C., Huang, H.C., 2012. Near-real-time global biomass burning emissions product from geostationary satellite constellation. J. Geophys. Res. 117, D14201. http://dx.doi.org/10.1029/2012JD017459.